ChemComm

COMMUNICATION

View Article Online
View Journal

Cite this: DOI: 10.1039/d0cc03149f

Received 1st May 2020,
Accepted 15th June 2020

DOI: 10.1039/d0cc03149f

rsc.li/chemcomm

Sensitive photoelectrochemical assay of Pb^{2+} based on DNAzyme-induced disassembly of the "Z-scheme" TiO_2/Au/CdS QDs system†

Leixia Meng, Mengyue Liu, Ke Xiao, Xiaohua Zhang, Cuicui Du and Jinhua Chen *

Herein, based on DNAzyme-induced disassembly of the "Z-scheme" TiO_2/Au/CdS QDs system, a facile and sensitive photoelectrochemical biosensor was developed for lead ion assay and a low detection limit of 0.13 pM was obtained.

As one of the most serious problems which have poisonous effects on human health and the environment, heavy metal pollution has garnered considerable attention.[1–3] Lead ions (Pb^{2+}), one of the typical heavy metal pollutants, are destructive to the nervous system, hematopoiesis, digestion, the kidneys, and the endocrine system as a result of its non-degradable and toxic features.[4] Thus, the detection of Pb^{2+} is of great significance for environmental protection, human health and food safety. Although various analytical techniques like atomic absorption/emission spectroscopy,[5,6] plasma mass spectrometry,[7] X-ray fluorescence spectrometry (XRF),[8] electrochemistry,[9] electrochemiluminescence[10] and fluorescence[11,12] have been reported, they still suffer from the drawbacks of expensive equipment, complicated operation procedures and requirement of professional technicians. In recent years, the photoelectrochemical (PEC) biosensor, a burgeoning and valuable analytical technology, has attracted significant interest because it possesses the characteristics of simplicity, high sensitivity, rapid responsivity, easy operation and low cost.[13,14] However, only a few studies have been reported the determination of Pb^{2+} based on the PEC method. For instance, Yuan *et al.* constructed a signal-on PEC biosensor for Pb^{2+} assay based on three-dimensional (3D) DNA networks.[15] However, it required a great deal of energy and time to accomplish the complicated and meticulous design of the 3D DNA networks, which was unbeneficial for practical application. Recently, Yuan *et al.* presented a wavelength distinguishable PEC biosensor with click reaction to detect triplex metal ions.[16] However, the detection limit was not low enough for sensitive assay due to the weak photocurrent signal of the photoelectric materials. Therefore, a facile and sensitive PEC biosensor is still urgently desirable for Pb^{2+} assay.

As is well-known, photoelectric materials play a very important role in a PEC biosensor. To enhance the photocurrent signal, numerous approaches, which mainly employ sundry noble metals (Au, Ag, *etc.*), semiconductors or organic materials as photosensitizers, have been proposed to inhibit the electron–hole recombination.[17–19] Recently, the emerging artificial "Z-scheme" system containing two-type photosensitizers has provided a new horizon to obtain a strong photocurrent signal.[20,21] In PEC biosensors, the "Z-scheme" system is generally constructed by an in-situ method.[22–24] For instance, Zhao *et al.* presented liposome-mediated *in situ* formation of the AgI/Ag/BiOI "Z-scheme" heterojunction, which was used for signal-on PEC bioanalysis.[23] On the other hand, there is only one reported work about a strategy to regulate the distance between two-type photosensitizers in the "Z-scheme" system so far. That is, Tang *et al.* developed a signal-off PEC bioassay based on the DNA hybridization-induced increase in the spatial distance between BiOCl and CdS in the "Z-scheme" system.[25] However, the sensitivity and detection limit were restricted because both of the two-type photosensitizers still existed on the surface of the sensing platform. Encouragingly, these studies inspired us to explore the disassembly of the "Z-scheme" system to improve the assay sensitivity of the signal-off PEC biosensor.

To date, RNA-cleaving DNA enzymes (DNAzymes) have been extensively applied in therapeutic, diagnostic and biosensing fields.[26–28] Compared to protein enzymes, DNAzymes possess certain advantages, such as better stability, more cost-effectiveness and non-specific adsorption.[28,29] DNAzymes can be activated by metal ions, resulting in the cleavage of the substrate strands into two fragments at a RNA (rA) position.[29–32] However, to the best of our knowledge, there is no report on PEC biosensors

State Key Laboratory of Chemo/Biosensing and Chemometrics, College of Chemistry and Chemical Engineering, Hunan University, Changsha, 410082, P. R. China. E-mail: chenjinhua@hnu.edu.cn; Fax: +86-731-88821848; Tel: +86-731-88821848

† Electronic supplementary information (ESI) available: DNA sequences used in this work; experimental section; material characterization; possible mechanism; optimization of experimental conditions; recovery test. See DOI: 10.1039/d0cc03149f

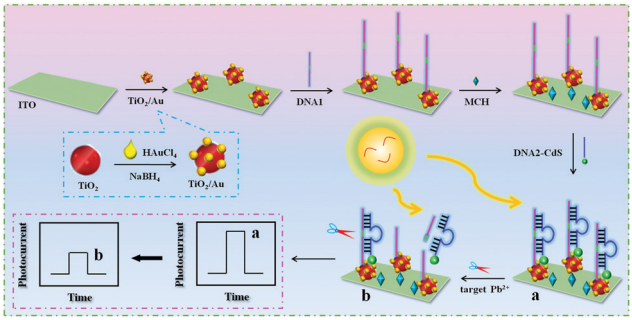

Scheme 1 Schematic diagram of the developed PEC biosensor for Pb^{2+} assay based on DNAzyme-induced disassembly of the "Z-scheme" TiO_2/Au/CdS QDs system.

based on the DNAzyme-induced disassembly of the "Z-scheme" system.

Herein, based on the Pb^{2+}-specific DNAzyme-induced disassembly of the "Z-scheme" TiO_2/Au/CdS QDs system, a facile and ultrasensitive PEC biosensor was for the first time established to detect Pb^{2+} (Scheme 1). A TiO_2/Au nanoparticle (NP)-modified indium tin oxide (ITO) electrode was utilized to immobilize the substrate strand DNA1 *via* the Au–S bond. Subsequently, the MPA-capped CdS QD-labeled catalytic strand DNA2 (DNA2-CdS QDs) was introduced into the electrode surface *via* hybridization, forming the "Z-scheme" TiO_2/Au/CdS QDs system and generating an enhanced PEC signal. Once the target Pb^{2+} was detected, the Pb^{2+}-specific DNAzyme was activated and then catalyzed the cleavage of DNA1, which induced the dissociation of the DNA1–DNA2 double helix and the disassembly of the "Z-scheme" TiO_2/Au/CdS QD system. As a result, the PEC signal decreased. The developed PEC biosensor exhibited excellent performance for Pb^{2+} assay with a wide linear response range of 0.5 pM–10 nM and a low detection limit of 0.13 pM (3σ), and good applicability in water and human serum samples, demonstrating great potential for practical applications in environment monitoring and clinical analysis. Also, this work provides a new strategy of DNAzyme-induced disassembly of the "Z-scheme" system to enhance the assay sensitivity of the signal-off PEC biosensing platform.

Fig. 1A displays the UV-vis absorption spectra of TiO_2 and TiO_2/Au hybrids. It is obvious that the light absorption intensity of TiO_2/Au hybrids (curve b) is stronger than that of pure TiO_2 (curve a) in the whole range of wavelengths, revealing that Au NPs improve the adsorption behaviour of TiO_2.[33] However, the absorption peak of Au NPs (about 500–600 nm) cannot be observed, indicating the absence of large nanoparticles.[34] On the other hand, structural characterization and crystalline phase analyses of TiO_2 and TiO_2/Au samples were carried out by powder X-ray diffraction (PXRD) and the results are shown in Fig. 1B. The characteristic peaks for TiO_2 at 25.3°, 37.8°, 48.1°, 54.0°, 55.1°, 62.9°, 69.1° and 75.2° correspond to the diffractions from the (101), (004), (200), (105), (211), (204), (220), and (215) planes of the anatase phase of TiO_2 (JCPDS 21-1272). Most importantly, the characteristic peaks appeared at 44.3°, 64.7° and 77.8° for TiO_2/Au hybrids, which are assigned to the

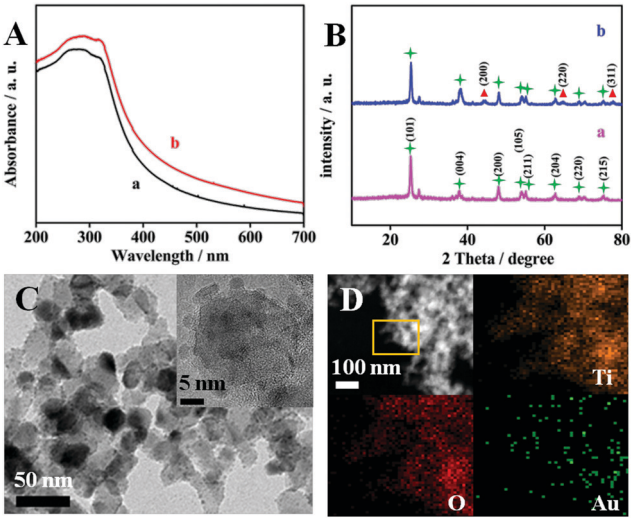

Fig. 1 (A) UV-vis absorption spectra and (B) PXRD patterns of TiO_2 (a) and TiO_2/Au (b). (C) TEM and (D) HAADF-STEM images and related elemental mapping images of Ti, O and Au of TiO_2/Au hybrids.

diffractions of the (200), (220), and (311) planes of Au, respectively. The characteristic peaks corresponding to Au show weak intensity, which is attributed to the small amount of Au.

As displayed in Fig. 1C, the mean size of the TiO_2/Au hybrids is approximately 25 nm, while the average size of Au NPs decorated on TiO_2 is about 3 nm. Additionally, high-angle annular dark-field scanning transmission electron microscopy (HAADF-STEM) was further utilized to investigate the composition of the TiO_2/Au hybrids. From Fig. 1D, according to the different colour contrasts of the picture, the elemental mappings of Ti, O and Au can be clearly observed, which certifies the existence of the Au element in TiO_2/Au hybrids. This suggests that the TiO_2/Au hybrids were successfully synthesized.

To investigate the electronic interaction in different components and the chemical states of the elements presented in the TiO_2/Au hybrids, X-ray photoelectron spectroscopy (XPS) analysis was carried out. As displayed in Fig. S1A (ESI†), the XPS survey spectrum indicates the presence of Ti, O, and Au elements in the TiO_2/Au hybrids, which is consistent with the above results of elemental mapping. The binding energies at 458.5 and 464.3 eV in the high-resolution Ti 2p spectrum (Fig. S1B, ESI†) are attributed to the spin–orbit splitting of the Ti 2p core level into $2p_{3/2}$ and $2p_{1/2}$, respectively. Compared to the original TiO_2, the binding energies are found to be positively migrated by about 0.1 eV, as a result of the movement in the Fermi level caused by the Fermi level equilibrium between TiO_2 and plasmonic Au NPs. This contributes to the electron transfer between Au NPs and the conduction band (CB) of TiO_2, which remains in line with the literature report.[35] From Fig. S1C (ESI†), two peaks at 83.2 and 86.8 eV are derived from Au $4f_{7/2}$ and Au $4f_{5/2}$, respectively. However, the position of Au $4f_{7/2}$ is obviously lower relative to the standard binding energy for metallic Au (84 eV). This reveals that Au NPs are in an electron-rich state or somewhat anionic in nature,[36] which again proves the electronic interaction between Au NPs and TiO_2, and the movement of electrons from Au NPs to

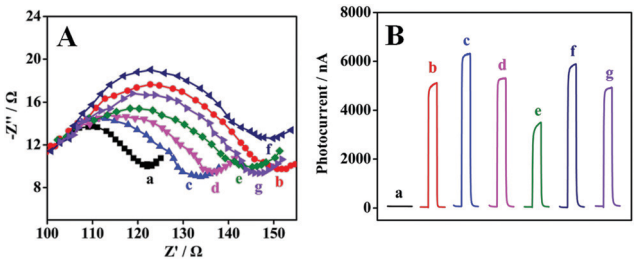

Fig. 2 (A) EIS characterization of the different electrodes in 0.1 M KCl aqueous solution containing 5 mM $[Fe(CN)_6]^{3-/4-}$ (1 : 1) in the frequency range from 0.01 Hz to 100 kHz at 5 mV. (B) Photocurrent signals of the different electrodes in 0.1 M PBS (pH 7.4) containing 0.1 M AA at −0.1 V. (a) ITO electrode, (b) ITO/TiO_2, (c) ITO/TiO_2/Au, (d) ITO/TiO_2/Au/DNA1, (e) ITO/TiO_2/Au/DNA1/MCH, (f) ITO/TiO_2/Au/DNA1/MCH/DNA2-CdS QDs, and (g) ITO/TiO_2/Au/DNA1/MCH/DNA2-CdS QDs incubated with Pb^{2+}.

TiO_2. Additionally, the surface atom content was obtained from the XPS results (Fig. S1D, ESI†), and the Au element is calculated to be only 0.72 atom%. In addition, the calculated TiO_2/Au mass ratio is 18 : 1. These results further indicate the successful decoration of Au NPs on TiO_2.

On the other hand, the results of high resolution transmission electron microscopy (HRTEM), Fourier transform infrared (FTIR) spectroscopy and UV-vis absorption spectroscopy shown in Fig. S2 (ESI†) reveal the successful preparation of MPA-capped CdS QDs and DNA2-CdS QDs.

Here, electrochemical impedance spectroscopy (EIS) was used to characterize the stepwise modification process of the biosensor. The semicircle diameter in the Nyquist plot of the EIS results is related to the interfacial charge transfer resistance (R_{ct}). As shown in Fig. 2A, the ITO electrode exhibits a small semicircle domain (curve a), suggesting a fast charge-transfer process. The R_{ct} value of the TiO_2-modified ITO electrode increases due to the semiconductor performance of TiO_2 (curve b). However, the R_{ct} value of the TiO_2/Au hybrid-modified ITO electrode (curve c) is smaller than that of the ITO/TiO_2 electrode. This should be attributed to the good conductive properties of Au NPs. Then, the immobilization of DNA1 on the electrode surface *via* the Au–S bond between the thiol groups on DNA1 and Au NPs on TiO_2 leads to an increase of the R_{ct} value (curve d) because of electrostatic repulsion between the negatively charged DNA and the anionic redox probe ($[Fe(CN)_6]^{3-/4-}$). The modifications of the electrode with MCH and DNA2-CdS QDs further increase the R_{ct} values (curves e and f), owing to the poor conductivity of MCH and DNA2-CdS QDs. However, when the above electrode is incubated with Pb^{2+} solution, the R_{ct} value of the electrode decreases (curve g). This should be attributed to the fact that the Pb^{2+}-specific DNAzyme is activated and then catalyzes the cleavage of DNA1, which induces the dissociation of the DNA1–DNA2 double helix and the release of DNA2-CdS QDs from the electrode surface. These results suggest the successful establishment of the proposed PEC biosensor according to Scheme 1.

PEC investigation was also carried out to further confirm each modification step during the preparation process of the electrode. As shown in Fig. 2B, there is no obvious photocurrent signal of the bare ITO electrode (curve a), and an anode photocurrent signal (5086 nA) can be observed (curve b) for the TiO_2-modified ITO electrode. While the ITO electrode is coated with TiO_2/Au hybrids, an enhanced photocurrent signal is obtained (6270 nA, curve c). This tendency can be explained by the localized surface plasmon resonance (LSPR) photosensitization effect of Au NPs, which results from the generated hot electron transfer of Au NPs to TiO_2 (Fig. S3A, ESI†).[17,37,38] Because of the electrostatic repulsion and blocking effect, the immobilizations of DNA1 and MCH in turn lead to the successive decreases of the photocurrents (5292 nA to 3470 nA, curves d to e). After the introduction of DNA2-CdS QDs on the electrode surface through hybridization between DNA1 and DNA2, the photocurrent remarkably increases from 3470 nA (curve e) to 5860 nA (curve f), as a result of the formation of the "Z-scheme" TiO_2/Au/CdS QDs system (Fig. S3B and S4, ESI†). The enhanced photocurrent provides a big initial signal, which is beneficial to the improvement of the analytical properties of the signal-off PEC biosensor. When Pb^{2+} exists, the Pb^{2+}-specific DNAzyme is activated and then catalyzes the cleavage of DNA1, leading to the dissociation of the DNA1–DNA2 double helix and the release of the DNA2-CdS QDs from the electrode surface. This decreases the PEC signal of the electrode (curve g, 4842 nA) because of the disassembly of the "Z-scheme" TiO_2/Au/CdS QDs system. The above results also indicate clearly that the developed PEC biosensor can be used in Pb^{2+} assay.

Under the optimal conditions (Fig. S5 and S6, ESI†), the developed PEC biosensing platform was used for Pb^{2+} assay. From Fig. 3A, it is worth noting that the photocurrent decreases with the increase of the concentration of Pb^{2+}. A linear relationship between the ΔI ($\Delta I = I_0 - I$, where I_0 and I represent the photocurrent values of the PEC biosensor in the absence and presence of Pb^{2+}, respectively) and the logarithm of the Pb^{2+} concentration is obtained in the range from 0.5 pM to 10 nM (Fig. 3B). The linear equation is ΔI (nA) = 513.4 $\log C_{Pb^{2+}}$ (pM) + 296.4 with a correlation coefficient of 0.9960 and the detection limit can be calculated to be 0.13 pM (3σ). In Table S2 (ESI†), the developed PEC biosensor shows a lower detection limit compared to other reported methods and much larger sensitivity than other PEC biosensors due to the DNAzyme-induced disassembly of the "Z-scheme" TiO_2/Au/CdS QDs system.

To evaluate the selectivity of the developed PEC biosensor, Mn^{2+}, Cu^{2+}, Ca^{2+}, Mg^{2+}, Cd^{2+}, and Zn^{2+} (100 nM for each of the metal ions) were used as interfering metal ions to replace Pb^{2+} (10 nM). As displayed in Fig. 3C, a significant photocurrent response ΔI ($\Delta I = I_0 - I$, where I_0 and I represent the photocurrent signals of the PEC biosensor in the absence and presence of metal ions, respectively) can be observed in the presence of Pb^{2+}, whereas no obvious changes are found for the interfering metal ions, indicating that the PEC biosensor shows excellent selectivity and can resist interference from other metal ions.

Additionally, the reproducibility of the PEC biosensor was assessed by measuring five modified electrodes with the same concentration of Pb^{2+} (10 nM) under the same conditions. From Fig. 3D, the relative standard deviation (RSD) is found to be 5.1%, suggesting good reproducibility. To further explore the stability, the ITO/TiO_2/Au/DNA1/MCH/DNA2-CdS QDs electrode

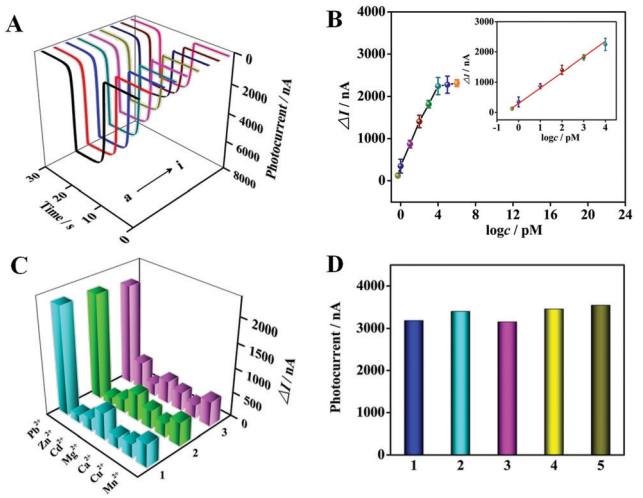

Fig. 3 (A) Photocurrent signals of the constructed PEC biosensor towards various concentrations of Pb^{2+}: 0, 0.5 pM, 1 pM, 10 pM, 100 pM, 1 nM, 10 nM, 100 nM, and 1000 nM (from a to i). (B) Calibration curve of the PEC biosensor for Pb^{2+} assay. (C) Specificity of the developed PEC biosensor for Pb^{2+} detection (with a concentration of 10 nM) over other interfering metal ions, including Mn^{2+}, Cu^{2+}, Ca^{2+}, Mg^{2+}, Cd^{2+}, and Zn^{2+} (100 nM for each metal ion). (D) Reproducibility of the developed PEC biosensor in the same batch.

was kept in a refrigerator at 4 °C for two weeks, and the photocurrent intensity retained about 95.6% of the initial value for Pb^{2+} detection (10 pM), demonstrating an acceptable stability of the PEC biosensor. Furthermore, the average recovery values for the added Pb^{2+} with 10 pM, 100 pM and 1000 pM are found to be 101.3%, 99.7%, 100.2% in tap water and 97.3%, 99.8% and 100.7% in diluted human serum samples, respectively (Table S3, ESI†). This indicates that the PEC sensor possesses good applicability in real samples.

In summary, a facile and sensitive PEC biosensor was developed for Pb^{2+} assay for the first time based on Pb^{2+}-specific DNAzyme-induced disassembly of the "Z-scheme" TiO_2/Au/CdS QDs system. The developed PEC biosensor shows good performance for Pb^{2+} assay with a wide linear response range of 0.5 pM–10 nM and a low detection limit of 0.13 pM (3σ). Furthermore, the PEC biosensor exhibits excellent selectivity, acceptable stability and reproducibility, and good applicability in water and human serum samples. By changing the heavy metal ion-specific DNAzyme, the developed sensing platform could be easily extended to detect other heavy metal ions. These features demonstrate that the developed PEC sensing strategy has great potential for practical applications in environment monitoring and clinical analysis.

This work was financially supported by the NSFC (21727810).

Conflicts of interest

There are no conflicts of interest to declare.

Notes and references

1 Z. J. Huang, J. M. Chen, Z. W. Luo, X. Q. Wang and Y. X. Duan, *Anal. Chem.*, 2019, **91**, 4806–4813.
2 Z.-B. Wen, W.-B. Liang, Y. Zhuo, C.-Y. Xiong, Y.-N. Zheng, R. Yuan and Y.-Q. Chai, *Chem. Commun.*, 2017, **53**, 7525–7528.
3 J. Li, W. W. Tu, H. B. Li, M. Han, Y. Q. Lan, Z. H. Dai and J. C. Bao, *Anal. Chem.*, 2014, **86**, 1306–1312.
4 J. Y. Zhuang, L. B. Fu, M. D. Xu, Q. Zhou, G. N. Chen and D. P. Tang, *Biosens. Bioelectron.*, 2013, **45**, 52–57.
5 M. W. Wensing, B. W. Smith and J. D. Winefordner, *Anal. Chem.*, 1994, **66**, 531–535.
6 R. Reuther, L. Jaeger and B. Allard, *Anal. Chim. Acta*, 1999, **394**, 259–269.
7 J. Woodhead, J. Hergt, S. Meffre, R. R. Large, L. Danyushevsky and S. Gilbert, *Chem. Geol.*, 2009, **262**, 344–354.
8 R. Sitko, P. Janik, B. Zawisza, E. Talik, E. Margui and I. Queralt, *Anal. Chem.*, 2015, **87**, 3535–3542.
9 Z. Z. Lin, Y. Chen, X. H. Li and W. H. Fang, *Analyst*, 2011, **136**, 2367–2372.
10 Y.-M. Lei, W.-X. Huang, M. Zhao, Y.-Q. Chai, R. Yuan and Y. Zhuo, *Anal. Chem.*, 2015, **87**, 7787–7794.
11 X.-H. Zhao, R.-M. Kong, X.-B. Zhang, H.-M. Meng, W.-N. Liu, W. H. Tan, G.-L. Shen and R.-Q. Yu, *Anal. Chem.*, 2011, **83**, 5062–5066.
12 H. Q. Wang, L. Yang, S. Y. Chu, B. H. Liu, Q. K. Zhang, L. M. Zou, S. M. Yu and C. L. Jiang, *Anal. Chem.*, 2019, **91**, 9292–9299.
13 C. M. Gao, H. H. Yu, L. N. Zhang, Y. H. Zhao, J. X. Xie, C. J. Li, K. Cui and J. H. Yu, *Anal. Chem.*, 2020, **92**, 2902–2906.
14 Z. Y. Wang, J. Liu, X. Y. Shi and Z. H. Dai, *Anal. Chem.*, 2019, **91**, 830–835.
15 L. J. Huang, L. Yang, C. C. Zhu, H. M. Deng, G. P. Liu and Y. L. Yuan, *Sens. Actuators, B*, 2018, **274**, 458–463.
16 H.-M. Deng, L.-J. Huang, Y.-Q. Chai, R. Yuan and Y.-L. Yuan, *Anal. Chem.*, 2019, **91**, 2861–2868.
17 J. Shu, Z. L. Qiu, S. Z. Lv, K. Y. Zhang and D. P. Tang, *Anal. Chem.*, 2018, **90**, 2425–2429.
18 Z. B. Luo, Q. G. Qi, L. J. Zhang, R. J. Zeng, L. S. Su and D. P. Tang, *Anal. Chem.*, 2019, **91**, 4149–4156.
19 X. Song, T. Hou, F. F. Lu, Y. Z. Wang, J. J. Liu and F. Li, *Chem. Commun.*, 2020, **56**, 1811–1814.
20 L. Favereau, A. Makhal, Y. Pellegrin, E. Blart, J. Petersson, E. Goransson, L. Hammarstrom and F. Odobel, *J. Am. Chem. Soc.*, 2016, **138**, 3752–3760.
21 P. Zhou, J. G. Yu and M. Jaroniec, *Adv. Mater.*, 2014, **26**, 4920–4935.
22 S.-Y. Yu, L.-P. Mei, Y.-T. Xu, T.-Y. Xue, G.-C. Fan, D.-M. Han, G. G. Chen and W.-W. Zhao, *Anal. Chem.*, 2019, **91**, 3800–3804.
23 H. M. Zeng, Y. L. Liu, Z. G. Xu, Y. J. Wang, Y. Q. Chai, R. Yuan and H. Y. Liu, *Chem. Commun.*, 2019, **55**, 11940–11943.
24 L. J. Zhang, Z. B. Luo, R. J. Zeng, Q. Zhou and D. P. Tang, *Biosens. Bioelectron.*, 2019, **134**, 1–7.
25 R. J. Zeng, Z. B. Luo, L. S. Su, L. J. Zhang, D. P. Tang, R. Niessner and D. Knopp, *Anal. Chem.*, 2019, **91**, 2447–2454.
26 M. Liu, D. R. Chang and Y. F. Li, *Acc. Chem. Res.*, 2017, **50**, 2273–2283.
27 L. D. Gu, W. L. Yan, H. J. Wu, S. H. Fan, W. Ren, S. J. Wang, M. S. Lyu and J. W. Liu, *Anal. Chem.*, 2019, **91**, 7887–7893.
28 W. H. Zhou, J. S. Ding and J. W. Liu, *Theranostics*, 2017, **7**, 1010–1025.
29 H. Y. Peng, A. M. Newbigging, Z. X. Wang, J. Tao, W. C. Deng, X. C. Le and H. Q. Zhang, *Anal. Chem.*, 2018, **90**, 190–207.
30 F. A. Wang, C.-H. Lu and I. Willner, *Chem. Rev.*, 2014, **114**, 2881–2941.
31 M. P. Robertson and A. D. Ellington, *Nat. Biotechnol.*, 1999, **17**, 62–66.
32 L. Gong, Z. L. Zhao, Y.-F. Lv, S.-Y. Huan, T. Fu, X.-B. Zhang, G.-L. Shen and R.-Q. Yu, *Chem. Commun.*, 2015, **51**, 979–995.
33 P. M. Da, W. J. Li, X. Lin, Y. C. Wang, J. Tang and G. F. Zheng, *Anal. Chem.*, 2014, **86**, 6633–6639.
34 J. P. Wu, K. L. Jiang, X. J. Wang, C. X. Wang and C. Zhang, *Microchim. Acta*, 2017, **184**, 1315–1324.
35 B. Tudu, N. Nalajala, K. P. Reddy, P. Saikia and C. S. Gopinath, *ACS Appl. Mater. Interfaces*, 2019, **11**, 32869–32878.
36 A. A. Melvin, K. Illath, T. Das, T. Raja, S. Bhattacharyya and C. S. Gopinath, *Nanoscale*, 2015, **7**, 13477–13488.
37 H. Li, F. Qin, Z. P. Yang, X. M. Cui, J. F. Wang and L. Z. Zhang, *J. Am. Chem. Soc.*, 2017, **139**, 3513–3521.
38 R. Y. Li, R. Yan, J. C. Bao, W. W. Tu and Z. H. Dai, *Chem. Commun.*, 2016, **52**, 11799–11802.

